A HERO'S DARK HORSE: DISCOVERY OF AN ULTRA-FAINT MILKY WAY SATELLITE IN PEGASUS

Dongwon Kim, Helmut Jerjen, Dougal Mackey, Gary S. Da Costa, and Antonino P. Milone
Research School of Astronomy and Astrophysics, The Australian National University, Mt Stromlo Observatory, via Cotter Rd, Weston, ACT 2611, Australia

Draft version April 16, 2015

ABSTRACT

We report the discovery of an ultra-faint Milky Way satellite galaxy in the constellation of Pegasus. The concentration of stars was detected by applying our overdensity detection algorithm to the SDSS-DR 10 and confirmed with deeper photometry from the Dark Energy Camera at the 4-m Blanco telescope. Fitting model isochrones indicates that this object, Pegasus III, features an old and metal-poor stellar population ($[Fe/H] \sim -2.1$) at a heliocentric distance of 205 ± 20 kpc. The new stellar system has an estimated half-light radius of $r_h = 78^{+30}_{-24}$ pc and a total luminosity of $M_V \sim -4.1 \pm 0.5$ that places it into the domain of dwarf galaxies on the size–luminosity plane. Pegasus III is spatially close to the MW satellite Pisces II. It is possible that the two might be physically associated, similar to the Leo IV and Leo V pair. Pegasus III is also well aligned with the Vast Polar Structure, which suggests a possible physical association.

Subject headings: Local Group – Milky Way, satellites: individual: Pegasus III

1. INTRODUCTION

Following the Sloan Digital Sky Survey (York et al. 2000), more recent wide-field imaging surveys such as the Stromlo Milky Way Satellite survey (Jerjen 2010), the Dark Energy Survey (The Dark Energy Survey Collaboration 2005), the Pan-STARRS 3π Survey (K. Chambers et al., in preparation), and the Survey of the Magellanic Stellar History (SMASH; PI D. Nidever) have been revealing new Milky Way companions including satellite galaxies (Koposov et al. 2015; Bechtol et al. 2015; Laevens et al. 2015; Martin et al. 2015) and star clusters (Belokurov et al. 2014; Laevens et al. 2014; Kim & Jerjen 2015; Kim et al. 2015). The new Milky Way companions, many of which are in the southern sky, share the properties of previously discovered ultra-faint stellar systems, such as low luminosities ($-8 \lesssim M_V \lesssim -1.5$) (Martin et al. 2008) and low metallicities $[Fe/H] < -2$ (Kirby et al. 2008; Norris et al. 2010; Simon et al. 2011; Koch & Rich 2014).

In this letter we report the detection of the new ultra-faint Milky Way satellite Pegasus III (Peg III) found in SDSS Data Release 10 and confirmed with deep DECam imaging (Sections 2 & 3). Peg III appears to be located at a heliocentric distance of ~ 205 kpc and have a half-light radius of ~ 78 pc (Section 4). In the last section we discuss the possible origin of the new satellite galaxy and conclude with our results.

2. DISCOVERY

The SDSS is a photometric and spectroscopic survey in the *ugriz* photometric bands to a depth of $r \sim 22.5$ magnitudes (York et al. 2000). Data Release 10 (DR10), publicly available on the SDSS-III Web site[1], covers $14,555 \deg^2$ mostly around the north Galactic pole (Ahn et al. 2014).

The new object was first flagged by our detection algorithm in the search for stellar overdensities over the exist-

ing SDSS catalog as described in Walsh et al. (2009) and Kim & Jerjen (2015). Briefly, we used isochrone masks based on the PARSEC stellar evolution models (Bressan et al. 2012) as a photometric filter to enhance the presence of old and metal-poor stellar populations relative to the Milky Way foreground stars. We then binned the R.A., DEC. positions of the filtered stars and convolved the density-map with a Gaussian kernel. Based on the density-map, we calculate the signal to noise ratios (S/Ns) of potential overdensities and measure their significance by comparing their S/Ns to those of random clusters in the residual background. Moving the isochrone masks over a range of distance moduli $(m-M)$ between 16 and 22 magnitudes, this process is repeated with different scales of bins and Gaussian kernels.

With this algorithm, we recovered all of the previously known MW companions in the SDSS coverage and found a few more promising candidates, one of which was reported in Kim & Jerjen (2015). The new object was detected with a significance of $\sim 7\sigma$ in the constellation of Pegasus.

3. FOLLOW-UP OBSERVATIONS AND DATA REDUCTION

Deeper follow-up observations of the Peg III field were conducted on during the night of 17th July 2014 using the Dark Energy Camera (DECam) at the 4-m Blanco Telescope located at Cerro Tololo Inter-American Observatory (CTIO) in Chile. DECam imager is equipped with a focal plane array containing sixty-two $2k \times 4k$ CCD detectors with a wide field of view (3.0 square degrees) and a pixel scale of $0''.27$ (unbinned). Under photometric conditions, we obtained 840 s exposures in g and 1050 s in r band, divided over dithered single exposures of 210 s. The average seeing during the observing was $1''.3$ in the g and $1''.1$ in the r band. The single exposure images were fully reduced and stacked through the DECam community pipeline (Valdes et al. 2014). We carried out weight-map combination, source extraction and PSF photometry with the use of WeightWatcher (Marmo & Bertin 2008)

dongwon.kim@anu.edu.au
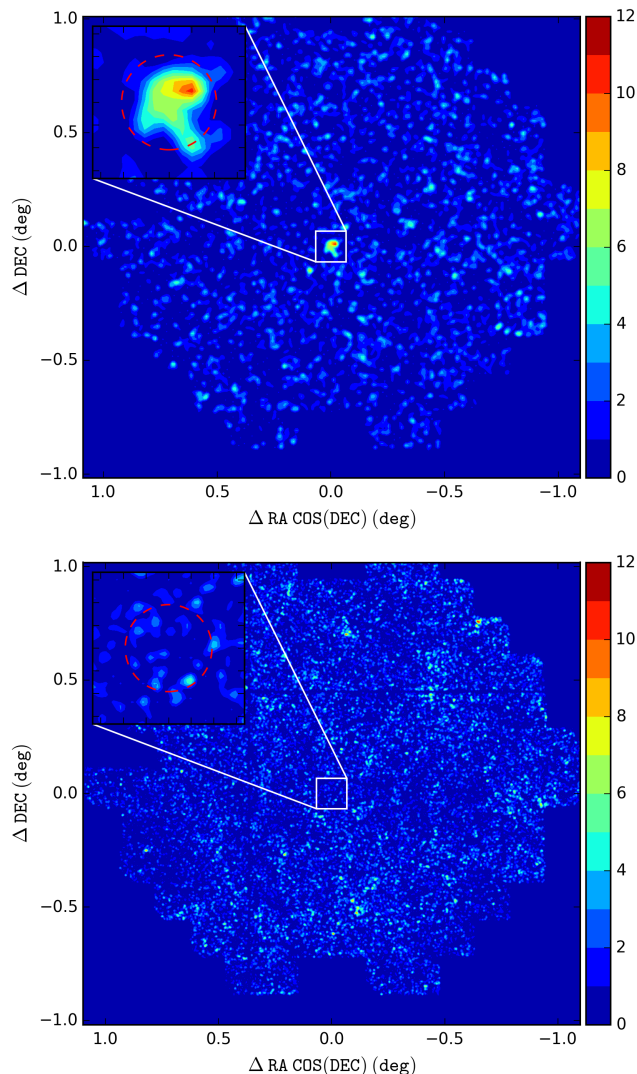[1] http://www.sdss3.org/dr10/

FIG. 1.— Upper panel: Density contours of candidate stars in the field of view of DECam that pass the photometric filter with a PARSEC isochrone of 13.5 Gyr and [Fe/H]= −2.1 (Bressan et al. 2012) at the distance modulus $(m − M) = 21.56$ magnitudes. The contours show the levels of star density in units of the standard deviation above the background. The dashed circle marks a radius of $2'.5$ (see Section 4 for details). Lower panel: Same as the upper panel but for all objects classified as galaxies. At the central region, there is no obvious overdensity coincident with that in the upper panel.

and SExtractor/PSFEx (Bertin & Arnouts 1996; Bertin 2011). For star/galaxy separation, we applied the threshold |SPREAD_MODEL| < 0.003 + SPREADERR_MODEL as described in Koposov et al. (2015). We then positionally matched the star-like objects with SDSS stars with a maximum radius of $1''.0$ using the STILTS software (Taylor 2005) . We used this catalog for the photometric calibration in the magnitude range $17.0 < r_0 < 21.0$ mag, between the saturation limit of the DECam and the 5σ limit of the SDSS. Finally, the magnitudes of the calibrated point sources were dereddened by means of the Schlegel et al. (1998) extinction maps and the extinction correction coefficients of Schlafly & Finkbeiner (2011).

The upper panel of Figure 1 shows the contour map of star density centred on Peg III in the field of view of DECam after the photometric filtering process using a

PARSEC isochrone of 13.5 Gyr and [Fe/H]= −2.1 (Bressan et al. 2012) at the distance modulus $(m−M) = 21.56$ magnitudes. High level density contours $(> 4\sigma)$ clearly define Peg III in the central region of the image and no other comparable overdensity in terms of S/N. Our algorithm recovers the overdensity with a significance of $\sim 10\sigma$ in the DECam data. The irregular shapes of the outer isophotes are likely due to the fact that we sample only the brightest red-giant branch (RGB) and horizontal branch (HB) stars in the system or that we see the signature of tidal disturbance. In the lower panel we present the same kind of contour map as shown in the upper panel but for all galaxy-like objects classified by the threshold SPREAD_MODEL > 0.003. There is no overdensity coincident with Peg III, ruling out the possibility of a background galaxy cluster.

4. CANDIDATE PROPERTIES

The left panel of Figure 2 shows the RA-DEC distribution of all stellar objects identified by SourceExtractor in the vicinity of Peg III. The middle left panel of Figure 2 shows the extinction-corrected CMD of stars within $2'.5$ (equal to the dashed circle in Figure 1) of the nominal centre of Peg III, and the middle right panel that of the foreground stars in the same manner as in Belokurov et al. (2010) from annulus defined by the outer radii of $8'.0$ and $8'.3$ covering the same area as the inner circle around Peg III. Finally, the right panel shows a field-subtracted Hess diagram, built on the CMDs in the middle. We note that Peg III shares a well defined RGB and blue-HB (BHB) with other distant MW satellite galaxies, namely, Leo V and Pisces II (Belokurov et al. 2008, 2010). The five BHB candidate stars clustering at $r_0 \sim 22$ mag and $(g − r)_0 \sim −0.1$ mag are highlighted as blue dots in the inner circle in the left panel of Figure 2. Fitting the horizontal branch of the PARSEC isochrone model yields an average heliocentric distance of ~ 205 kpc.

To derive the central position α and δ, ellipticity ϵ, position angle θ and half-light radius r_h, we employed a maximum-likelihood algorithm similar to the procedure described in Martin et al. (2008) with the stars that passed the photometric filter. We obtained a half-light radius of $1.3^{+0.5}_{-0.4}$ arcmin, or 78^{+30}_{-24} pc adopting a heliocentric distance of 205 kpc. The radial density profile with the best-fitting exponential model is presented in Figure 3.

We estimate the total luminosity of Peg III in analogy to Walsh et al. (2008) as follows. First, we calculate the total number of Peg III stars N_* within the photometric limit by integrating the best-fitting exponential profile shown in Figure 3. We use the ratio of the total number of stars N_* to the probability density of a normalised theoretical luminosity function (LF) in the same magnitude range. Using this ratio, we scale the theoretical LF to the star number density as a function of r magnitude. We then integrate the scaled LF taking into account the missing flux beyond the lower limit of our photometry and obtain a total luminosity $M_r = −4.23$ mag based on the initial mass function by Kroupa (2001) and PARSEC isochrone for a 13.5 Gyr old stellar population with [Fe/H]= −2.1. From the $V − r = 0.17$ mag luminosity weighted mean color for the model isochrone we derive the corresponding V-band luminosity $M_V = −4.1$ mag. Since this method relies on total star counts instead of
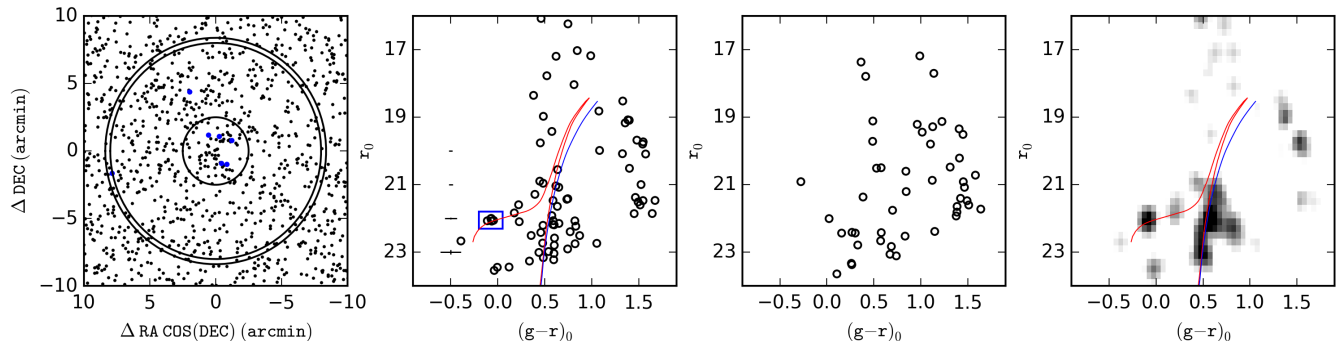
FIG. 2.— DECam view of Peg III. Left panel: Distribution of all objects classified as stars in a $20' \times 20'$ field that shares the central coordinates with Figure 1. The circles mark a radius of 2.5 (equal to the dashed circle in Figure 1), 8.0 and 8.3 respectively. The blue dots mark the seven BHB stars that fall into the color-magnitude range $-0.20 < (g-r)_0 < 0.05$ and $21.80 < r_0 < 22.30$, illustrated as a blue box in the next panel. Middle left panel: CMD of stars lying within the inner circle, dominated by the candidate stars of the dwarf galaxy. Middle right panel: Comparison CMD of stars lying in the annulus defined by the two outer circles, dominated by foreground stars. Right panel: Field-subtracted Hess diagram, the inner CMD minus the comparison CMD, showing an excess of stars at the locations of the BHB and RGB of Peg III. The best-fitting PARSEC (red) isochrone of age 13.5 Gyr and [Fe/H]=-2.1 and Dartmouth (Dotter et al. 2008) (blue) isochrone of age 14.2 Gyr and [Fe/H]$= -2.3$ are overplotted at a distance of 205 kpc.
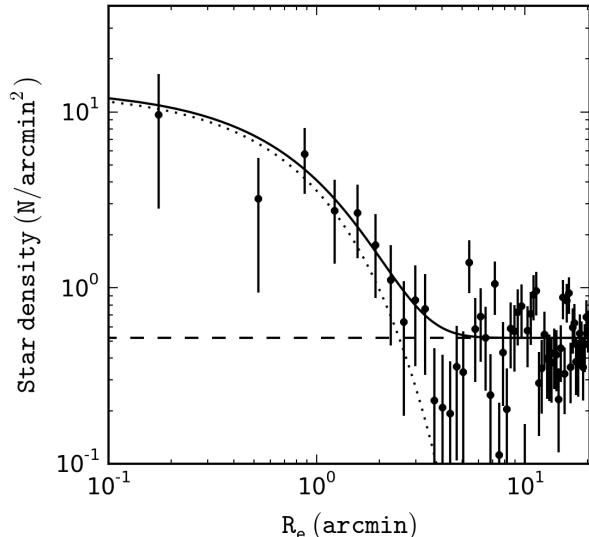
FIG. 3.— Radial stellar density profile of Peg III. R_e is the elliptical radius. Overplotted are the best exponential model based on the parameters in Table 1 (dotted), the contribution of foreground stars (dashed) and the combined fit (solid). The error bars were derived from Poisson statistics.

individual flux, the inclusion or exclusion of a single RGB in the system carries large uncertainties up to ~ 0.5 mag. Hence, a realistic estimate of the total luminosity of Peg III is $M_V = -4.1 \pm 0.5$. All derived parameters are summarised in Table 1.

5. DISCUSSION AND CONCLUSION

We report the discovery of a new ultra-faint Milky Way satellite, Peg III. The satellite hosts a typical old, metal-poor stellar population as it is observed in many other Milky Way satellite galaxies. Its large half-light radius (~ 78 pc) and luminosity (-4.1 ± 0.5) puts Peg III among other systems classified as ultra-faint dwarf galaxies in the size-luminosity parameter space as shown in Figure 4. In particular, these physical properties of Peg III are very similar to those of previously known remote MW satellites such as Leo IV ($d_\odot = 154 \pm 5$ kpc, $r_h = 206^{+36}_{-31}$ pc; Moretti et al. 2009), Leo V ($d_\odot = 196 \pm 15$ kpc, $r_h = 65 \pm 30$ pc; Sand et al. 2012) and

TABLE 1
PROPERTIES OF PEG III

Parameter	Value	Unit
α_{J2000}	22 24 22.6±1.0	h m s
δ_{J2000}	+05 25 12±14	° ′ ″
l	69.852	deg
b	−41.813	deg
$(m-M)$	21.56 ± 0.20	mag
$d_\odot$	205 ± 20	kpc
r_h	$78^{+30\ a}_{-24}$	pc
ϵ	$0.46^{+0.18}_{-0.27}$	
θ	133 ± 17	deg
$M_{tot,V}$	-4.1 ± 0.5	mag

[a] Adopting a distance of 205 kpc

Pisces II ($d_\odot = 183 \pm 15$ kpc, $r_h = 58 \pm 10$ pc; Sand et al. 2012). We note that we could have overestimated the half-light radius of Peg III due to the sampling of stars limited to RGB/HB and field-contamination. Deeper photometry down to the main-sequence stars tends to give smaller half-light radii as shown in previous studies (e.g. Leo V in de Jong et al. 2010; Sand et al. 2012). However, even if the true size is only half of the current estimate, Peg III would be still found in the region where ultra-faint dwarf galaxies populate in the size-luminosity parameter space.

It is interesting to note that Peg III and Pisces II are separated only by 8.5 deg on the sky and have fairly similar distances (205 ± 20 kpc and 183 ± 15 kpc). The spatial separation of the two satellite galaxies is ~ 30 kpc. A similar situation has already been encountered with the Leo IV and Leo V pair (de Jong et al. 2010). This suggests that Peg III and Pisces II could be associated with each other, although a velocity measurement will be required to confirm or reject this idea. As for the Leo IV– Leo V pair they might be related to a single disrupting or disrupted progenitor. It might be a pure coincidence but the Peg III–Pisces II and Leo IV–Leo V pairs are almost diametrically opposite (in fact 162 deg) in the sky, and have almost the same angular separation of ~ 90 deg from the barycenter of the Magellanic Clouds, ie. 88 deg and 103 deg, respectively.

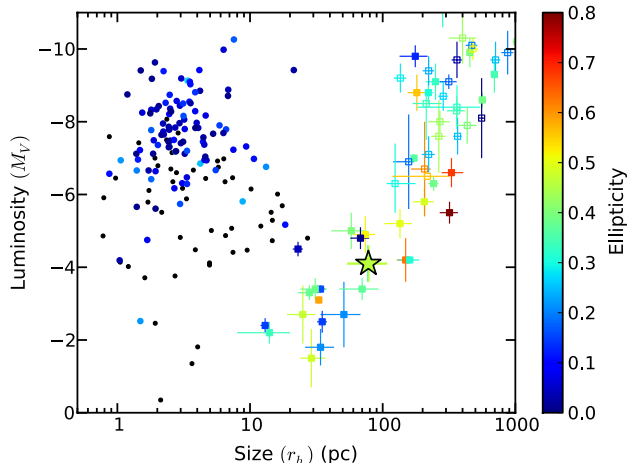With an angular distance of ~ 13 deg, Peg III lies also

Fig. 4.— The position of Peg III on the size-luminosity plane, marked with a star outlined in black. Also shown are all Milky Way globular clusters (filled circles), and the presently-known dwarf spheroidal satellites of the Milky Way (filled squares) and M31 (open squares). All points are colour-coded by ellipticity; those globular clusters lacking an ellipticity measurement are marked in black. Peg III clearly occupies the region inhabited by ultra-faint dwarf satellites of the Milky Way, and it has a comparable ellipticity to many of these objects. We note that Peg III directly falls on top of Coma Berenices, which is therefore invisible on this plot. Measurements for the globular clusters were taken from Harris (1996, and 2010 edition); those for the Milky Way dwarfs from McConnachie (2012), Belokurov et al. (2014),Laevens et al. (2014, 2015), Kim et al. (2015), Koposov et al. (2015), Bechtol et al. (2015), and Martin et al. (2015); and those for the M31 dwarfs from McConnachie (2012), and Martin et al. (2013a,b) In the case where more than one independent set of luminosity and/or structural measurements exists for an object, we adopt their weighted mean.

close the vast polar structure (VPOS), a planar arrangement defined by the 27 previously known Milky Way satellite galaxies, including the Magellanic Clouds, perpendicular to the MW disk (Kroupa et al. 2005; Metz et al. 2007, 2009; Kroupa et al. 2010; Pawlowski et al. 2012). The majority of recently discovered Milky Way satellite candidates in the southern hemisphere (Koposov et al. 2015; Bechtol et al. 2015) are also well aligned with the VPOS (Pawlowski et al. 2015, in preparation). The origin of that plane is still a matter of debate. It could be the result of a major galaxy collision that left debris in form of tidal dwarfs and star clusters along the orbit (Pawlowski et al. 2013). Peg III might be part of that debris.

REFERENCES

Ahn, C. P., Alexandroff, R., Allende Prieto, C., et al. 2014, ApJS, 211, 17

Bechtol, K., Drlica-Wagner, A., et al. 2015, arXiv:1503.02584

Belokurov, V., Zucker, D. B., Evans, N. W., et al. 2007, ApJ, 654, 897

Belokurov, V., Walker, M. G., Evans, N. W., et al. 2008, ApJ, 686, L83

Belokurov, V., Walker, M. G., Evans, N. W., et al. 2010, ApJ, 712, L103

Belokurov, V., Irwin, M. J., Koposov, S. E., et al. 2014, MNRAS, 441, 2124

Bertin, E., & Arnouts, S. 1996, A&AS, 117, 393

Bertin, E. 2011, Astronomical Data Analysis Software and Systems XX, 442, 435

Bressan, A., Marigo, P., Girardi, L., et al. 2012, MNRAS, 427, 127

de Jong, J. T. A., Martin, N. F., Rix, H.-W., et al. 2010, ApJ, 710, 1664

Dotter, A., Chaboyer, B., Jevremović, D., et al. 2008, ApJS, 178, 89

Harris, W. E. 1996, AJ, 112, 1487

Jerjen, H. 2010, Advances in Astronomy, 2010, 434390

Kim, D., & Jerjen, H. 2015, ApJ, 799, 73

Kim, D., Jerjen, H., Milone, A. P., Mackey, D., & Da Costa, G. S. 2015, arXiv:1502.03952

Kirby, E. N., Simon, J. D., Geha, M., Guhathakurta, P., & Frebel, A. 2008, ApJ, 685, L43

Koch, A., & Rich, R. M. 2014, arXiv:1408.3628

Kroupa, P. 2001, MNRAS, 322, 231

Kroupa, P., Theis, C., & Boily, C. M. 2005, A&A, 431, 517

Kroupa, P., Famaey, B., de Boer, K. S., et al. 2010, A&A, 523, A32

Koposov, S. E., Belokurov, V., Torrealba, G., & Wyn Evans, N. 2015, arXiv:1503.02079

Laevens, B. P. M., Martin, N. F., Sesar, B., et al. 2014, ApJ, 786, L3

Laevens, B. P. M., Martin, N. F., Ibata, R. A., et al. 2015, arXiv:1503.05554

Marmo, C., & Bertin, E. 2008, Astronomical Data Analysis Software and Systems XVII, 394, 619

Martin, N. F., de Jong, J. T. A., & Rix, H.-W. 2008, ApJ, 684, 1075

Martin, N. F., Slater, C. T., Schlafly, E. F., et al. 2013, ApJ, 772, 15

Martin, N. F., Schlafly, E. F., Slater, C. T., et al. 2013, ApJ, 779, LL10

Martin, N. F., Nidever, D. L., Besla, G., et al. 2015, arXiv:1503.06216

McConnachie, A. W. 2012, AJ, 144, 4

Metz, M., Kroupa, P., & Jerjen, H. 2007, MNRAS, 374, 1125

Metz, M., Kroupa, P., & Jerjen, H. 2009, MNRAS, 394, 2223

Moretti, M. I., Dall'Ora, M., Ripepi, V., et al. 2009, ApJ, 699, L125

Norris, J. E., Yong, D., Gilmore, G., & Wyse, R. F. G. 2010, ApJ, 711, 350

Pawlowski, M. S., Pflamm-Altenburg, J., & Kroupa, P. 2012, MNRAS, 423, 1109

Pawlowski, M. S., Kroupa, P., & Jerjen, H. 2013, MNRAS, 435, 1928

Sand, D. J., Strader, J., Willman, B., et al. 2012, ApJ, 756, 79

Schlafly, E. F., & Finkbeiner, D. P. 2011, ApJ, 737, 103

Schlegel, D. J., Finkbeiner, D. P., & Davis, M. 1998, ApJ, 500, 525

Simon, J. D., Geha, M., Minor, Q. E., et al. 2011, ApJ, 733, 46

Taylor, M. B. 2005, Astronomical Data Analysis Software and Systems XIV, 347, 29

The Dark Energy Survey Collaboration 2005, arXiv:astro-ph/0510346

Valdes, F., Gruendl, R., & DES Project 2014, Astronomical Data Analysis Software and Systems XXIII, 485, 379

Walsh, S. M., Willman, B., Sand, D., et al. 2008, ApJ, 688, 245

Walsh, S. M., Willman, B., & Jerjen, H. 2009, AJ, 137, 450

York, D. G., Adelman, J., Anderson, J. E., Jr., et al. 2000, AJ, 120, 1579